

Fast measurement of picoamp plasma flows using trapped electron clouds

A. A. Kabantsev^{a)} and C. F. Driscoll

Department of Physics, University of California at San Diego, La Jolla, California 92093

(Presented on 19 April 2004; published 5 October 2004)

We demonstrate that magnetized electron clouds can diagnose picoamp ion currents (or equivalent neutralized plasma flows) on a kHz time scale. This could be used to measure the dynamics of neutral plasma losses to the walls, e.g., along divertor field lines. In essence, a current passing through an electron cloud in a Penning trap transfers angular momentum to the cloud, driving an easily measured orbital “diocotron” instability (from ion currents) or orbital damping (from electron currents). With neutralized plasma flows, the predominant effect is from the lower velocity (i.e., higher density) charge species. Experiments with electron, ion, and neutralized currents have fully characterized this collective (collisionless) electrostatic interaction, and demonstrate the picoamp and kHz resolutions. © 2004 American Institute of Physics. [DOI: 10.1063/1.1788860]

I. INTRODUCTION

Measurements of the fast dynamics of quasineutral plasma flows and/or small ion currents along magnetic field-lines are of great importance in the understanding of plasma behavior in various confinement devices. However, it is still a challenging task for several reasons. Conventional ways to monitor the currents, such as measuring the current-induced magnetic field fluctuations, tend to have inadequate sensitivity to low currents in strongly magnetized plasmas. Another strict limitation is that fully neutralized flows are intangible to the field-inductive or charge-collective techniques.

Here, we demonstrate a novel experimental approach based on monitoring the instabilities which occur when the currents couple to transverse mode of an electron plasma gauge. In essence, a current passing through an electron cloud (confined in a small Penning trap) transfers angular momentum to the cloud, driving an easily measured orbital “diocotron” instability (from ion currents) or orbital damping (from electron currents). Since the angular momentum transfer is not only charge dependent but also mass dependent, the method allows nonperturbative measurements of equivalent currents even for completely neutralized plasma flows.

II. EXPERIMENTAL SETUP

The basic arrangements for the experiments are shown schematically in Fig. 1. The confinement geometry is cylindrical and the entire system is immersed in a nearly uniform axial magnetic field of $1 \leq B \leq 15$ kG. Electrons are thermally emitted from a negatively biased filament towards the grounded grid. Electrons stream along magnetic field lines into the grounded central section of radius $R_w = 3.5$ cm, and are reflected by a negative potential applied to the confinement ring at the right end of the trap. Gating the injection ring negative traps the electron column. The electrons reside

in the central section, with axial confinement provided by the end cylinders and radial confinement provided by the axial magnetic field.

The electron column $\mathbf{E} \times \mathbf{B}$ drift rotates, due to the strong radial electric field resulting from the unneutralized space charge. A few of the central cylinders are divided into angular sectors that can be used to launch or detect waves having azimuthal ($e^{im\theta}$) dependence. The total charge of the confined electron column Q_e is typically measured by gating the right confinement ring to the ground and dumping all electrons on the positively biased end plate. The plasmas have typical density $n_e = 10^7$ cm⁻³ over a radius $R_e = 1.5$ cm. The temperature can be measured by passing the dumped electrons through a velocity analyzer. The typical electron temperature is in the range of 0.5 eV, giving a Debye length of $\lambda_D \approx 0.2$ cm. This column is a pure electron plasma by the criterion that $\lambda_D \ll R_e$. These pure electron plasmas have exceptional confinement properties¹ and can be contained for hours.²

For calibration purposes, transiting ion and/or electron currents can be readily produced in the filament-grid region. Filament electrons are accelerated by the positively biased grid, and then are reflected by the more negative injection ring. If their energy is above the ionization potential of the background gas (here H₂) then an ion current will be extracted from the grid region by the negative plasma potential. The magnitude of the ion current is controlled by the grid-filament bias (up to the maximum of ionization cross section) and by the background pressure. Alternatively, making the filament bias closer to the injection ring potential (and well below the plasma potential) allows some electrons to penetrate through the injection gate, forming an electron beam that passes through the plasma column. As the filament bias is progressively decreased, this electron current increases, first matching the ion current, then becoming dominant. All the currents passing through the plasma column are monitored on a biased end plate.

^{a)}Electronic mail: aakpla@physics.ucsd.edu

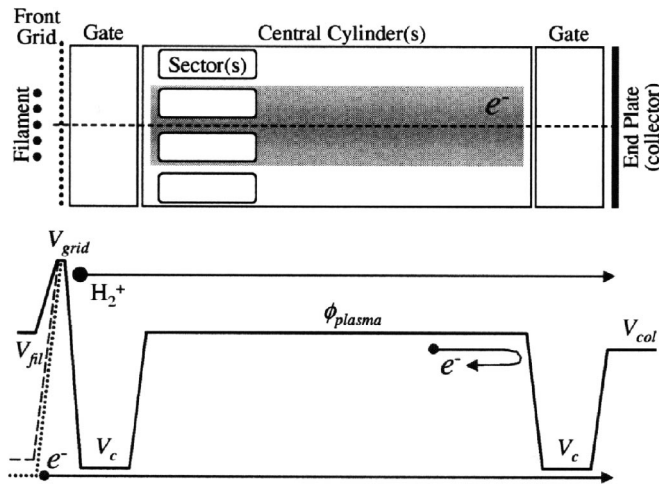


FIG. 1. Apparatus.

III. THEORETICAL EXPECTATIONS

Pure electron plasmas contained in such axisymmetric geometry have exceptional confinement properties, as compared with neutral plasmas. One reason for this is that angular momentum conservation strongly constrains the radial transport.¹ Like-particle interactions, however complex and nonlinear, cannot cause the plasma to expand radially, because the total canonical angular momentum must be conserved. The total canonical angular momentum L_θ is the sum of a mechanical and a vector-potential contribution, as

$$L_\theta = \sum_j \left[m_e v_{\theta j} r_j + \frac{eB_z}{2c} (R_w^2 - r_j^2) \right].$$

Here r_j is the distance of electron j from the axis, $v_{\theta j}$ is its θ velocity, m_e is its mass, and the summation is over all particles. For kiloGauss fields and electronVolt energies, the mechanical contribution (first term) is several orders less than the electromagnetic part, and can be safely neglected. If there are no external couplings applying torques and hence changing the angular momentum, the constraint on radial positions is then $\sum_j r_j^2 = \text{constant}$, which implies that there can be no bulk expansion of the electron plasma.

Here, we consider “diocotron” modes on the nominally cylindrical electron plasma, with $m_\theta = 1, 2, \dots$ and $k_z = 0$. The $m_\theta = 1$ mode represents a displacement D_1 of the column off the trap axis, with resulting $\mathbf{E} \times \mathbf{B}$ drift orbit of the column around the axis. The $m_\theta = 2$ mode represents an elliptical distortion (magnitude D_2) of the centered column. With these modes excited, the angular momentum summation can be written

$$\sum_j r_j^2 = R_0^2 + \sum_m D_m^2.$$

The column radius R_0 and diocotron wave amplitude D_m are thus free to change while conserving $\sum_j r_j^2$, as long as $R_0 dR_0 + \sum_m D_m dD_m = 0$.

An external particle beam which transits through the electron plasma will, in general, gain or lose some angular momentum; and the electron plasma will lose or gain a corresponding amount. For simplicity, here we assume that the charge particle linear density of this external flow is small

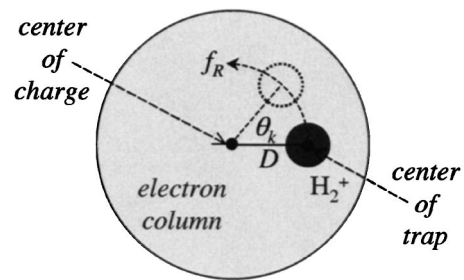


FIG. 2. Schematics of the drift dynamics.

compared to the linear density of the electron column. The heuristic argument can be made that collective beam–plasma interactions will change the wave part of angular momentum, while binary particle collisional interactions will contribute predominantly to a change in R_0 . Experimentally we have confirmed that in our relatively collisionless system, the main change occurs to the wave amplitude D_m .

Consider the visually simple case of the fundamental $m_\theta = 1$ diocotron mode, shown schematically in Fig. 2. The center of charge of the electron column is displaced a distance D from the center of the trap. Consider a transiting H_2^+ ion centered in the trap. After entering into the electron column, the charged particles begin their $\mathbf{E} \times \mathbf{B}$ drift around the axis of the electron column, rotating at frequency f_R . Thus, during the passage time $t_k = L_e / v_k$, the ions acquire an angle $\theta_k = 2\pi f_R L_e / v_k$, which corresponds to a radial displacement $2D \sin(\theta_k/2)$ with respect to the geometrical axis of the trap. The subscript k represents the different velocity components of charged particle flows. It is instructive to note that these time-of-flight angles θ_k may be dramatically different for the slow and fast components. In the case of quasineutral plasma flows ($I_e \approx -I_i$) and $f_R L_e / v_i \leq 1/2$, the net effect of electron current is negligible, i.e., $\mathcal{O}(m_e/M_i)$, so this technique measures only the ion part of these flows.

For a uniform rotation frequency, $f_R = ec n_e / B_z$, we can express the acquired angle as $\theta_k \approx (2|Q_e|/B_z R_e^2)(c/v_k)$. The angular momentum continuously carried off by passing particles is thus $\dot{L}_\theta = (B/2c) \sum_k I_k 4D^2 \sin^2(\theta_k/2)$. This torque transfer between the passing charged particles and the electron column causes the diocotron mode to grow at a rate

$$\gamma = \sum_k \frac{I_k}{|Q_e|} 2 \sin^2 \left[\left(\frac{Q_e}{B_z R_e^2} \right) \left(\frac{c}{v_k} \right) \right].$$

For ions not axially centered in the trap, a θ and v average gives growth of essentially the same magnitude.

Thus, while the sign of particles carrying electric current determines the sign of their contribution to the effect (i.e., growth or damping of diocotron modes), its magnitude is defined both by the normalized current term I_k/Q_e and by the oscillating function of the angular momentum recoil $\sin^2[(Q_e/B_z R_e^2)(c/v_k)]$. To maximize sensitivity of this technique, the argument in the square brackets has to be a substantial fraction of $\pi/2$. This can be achieved by adjustments of the guiding magnetic field B_z , the total electron charge in the cell Q_e , and the electron column radius R_e . In addition, by varying B_z it is possible not only to measure the total

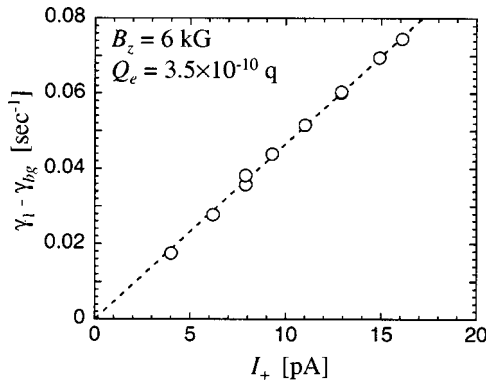


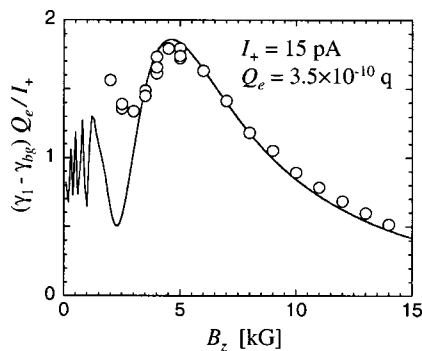
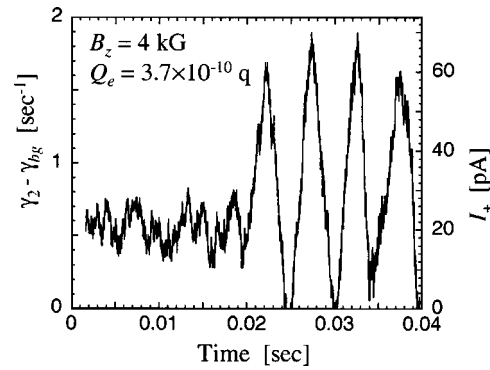
FIG. 3. Net growth rate vs ion current.

current of charged particle flows, but also separately obtain their typical average velocity $\langle v_k \rangle$ and the linear charge density $\sum_k I_k / \langle v_k \rangle$.

IV. EXPERIMENTAL RESULTS

Figure 3 shows growth rate γ_1 of the $m_\theta=1$ diocotron mode versus ion current. Here, every point represents the dc current-induced growth rate averaged over a 10 s time span. In general, there is a small background growth/damping of the diocotron waves γ_{bg} even in the absence of any beam currents; here, $\gamma_{bg} \sim 0.01 \text{ s}^{-1}$. This represents resistive wall destabilization,³ asymmetry-induced trapped-particle mediated damping,⁴ damping from rotational pumping,⁵ and spatial Landau resonance damping for broad $n_e(r)$ profiles.⁶ Ion currents in as low as 1 pA can be easily measured.

Figure 4 shows the magnetic field dependence of γ_1 due to the oscillating term of the angular momentum recoil,

FIG. 4. B dependence of the normalized current-induced growth rate (oscillations of angular momentum recoil).FIG. 5. Growth rate of the $m_\theta=2$ diocotron mode for 20 pA dc at and 60 pA at 0.2 kHz ac ion currents.

$\sin^2[(Q_e/B_z R_e^2)(c/v_k)]$. The high field shows a perfect $1/B_z^2$ dependence, while at the low B_z end there is a strong interference between components with different v_k . The best fit curve for a simple ion energy distribution mode gives the average ion energy $\langle E_k \rangle \approx 33 \text{ eV}$, which is in good correspondence to that measured using retarding potential at the end (collector) plate.

This beam-induced growth may be measured on a millisecond time scale, as shown in Fig. 5. Here, a nominally steady 20 pA ion current is injected for 20 ms, followed by a 60 pA ion current modulated at 0.2 kHz. Here we have excited and monitored the growth of the $m_\theta=2$ diocotron mode ($f_2 \approx 62 \text{ kHz}$) instead of the fundamental mode ($f_1 \approx 8 \text{ kHz}$). In principle, the higher-order azimuthal modes ($m_\theta=2, 3, 4, \dots$) allow significantly better time resolution, since $f_m \approx (m_\theta - 1)f_2$. However, since these modes are subject to the spatial Landau damping,⁶ their practical use is limited to the rare case of nearly “top-hat” radial density profile $n_e(r)$.

ACKNOWLEDGMENT

This work was supported by National Science Foundation Grant No. PHY9876999.

¹T. M. O’Neil, Phys. Fluids **23**, 2216 (1980).

²C. F. Driscoll, K. S. Fine, and J. H. Malmberg, Phys. Fluids **29**, 2015 (1986).

³W. D. White, J. H. Malmberg, and C. F. Driscoll, Phys. Rev. Lett. **49**, 1822 (1982).

⁴A. A. Kabantsev, J. H. Yu, R. B. Lynch, and G. F. Driscoll, Phys. Plasmas **10**, 1628 (2003).

⁵B. P. Cluggish and G. F. Driscoll, Phys. Rev. Lett. **74**, 4213 (1995).

⁶R. J. Briggs, J. D. Daugherty, and R. H. Levy, Phys. Fluids **13**, 421 (1970).